Infrared all-dielectric Kerker metasurfaces

KEBIN FAN,[1,2,5] **ILYA V. SHADRIVOV,**[3] **ANDREY E. MIROSHNICHENKO,**[4] **AND WILLIE J. PADILLA**[1,6]

[1]*Department of Electrical and Computer Engineering, Duke University, Box 90291, Durham, NC 27708, USA*

[2]*Present address: School of Electronics Science and Engineering, Nanjing University, Nanjing 210023, China*

[3]*Centre of Excellence on Transformative Meta-Optical Systems (TMOS) at Nonlinear Physics Centre, Research School of Physics, The Australian National University, Canberra, ACT 2601, Australia*

[4]*School of Engineering and Information Technology, University of New South Wales, Canberra, ACT 2600, Australia*

[5]*kebin.fan@nju.edu.cn*

[6]*willie.padilla@duke.edu*

Abstract: The unidirectional scattering of electromagnetic waves in the backward and forward direction, termed Kerkers' first and second conditions, respectively, is a prominent feature of sub-wavelength particles, which also has been found recently in all-dielectric metasurfaces. Here we formulate the exact polarizability requirements necessary to achieve both Kerker conditions simultaneously with dipole terms only and demonstrate its equivalence to so-called "invisible metasurfaces". We further describe the perfect absorption mechanism in all-dielectric metasurfaces through development of an extended Kerker formalism. The phenomena of both invisibility and perfect absorption is shown in a 2D hexagonal array of cylindrical resonators, where only the resonator height is modified to switch between the two states. The developed framework provides critical insight into the range of scattering response possible with all-dielectric metasurfaces, providing a methodology for studying exotic electromagnetic phenomena.

The electromagnetic scattering of waves from individual or arrays of particles occurs when the field produced by the sample cannot be easily described using simple theories of reflection and refraction. Complexity arises because the incident electromagnetic waves may induce multi-poles within the object, thereby producing additional fields which then contribute to the total scattered fields [1,2]. However, if the scatterers are of infinitesimal thickness, consisting of planar 2D metallic structures, then the resonators strictly only support an electrical response and thus their scattering is limited to be identical in both the forward and backward directions [3]. In order to overcome this fundamental limitation, while at the same time minimizing complexity, past studies used magnetic and electric resonances in order to provide more scattering versatility [3–7]. For example, a planar array of sub-wavelength scatters may be arranged to reduce interference effects through spatial overlap of the electric and magnetic dipoles, allowing designed scattering responses with suppressed backward scattering by Huygens principle [8–11].

A rational design approach is enabled by all dielectric metasurfaces which can provide varied and designer scattering responses [12]. All-dielectric metasurfaces have demonstrated exotic electromagnetic properties including Huygens' lenses [9,11], reflectarrays [13–15], zero-rank absorbers [16], coherent perfect absorbers [16–18], and bound-states-in-the-continuum [19–22]. It was realized that through proper tuning of the electric and magnetic dipole responses a condition of zero back scattering can be obtained – termed Kerker's first condition – while a different arrangement enables zero forward scattering – called Kerker's second condition [23]. All-dielectric based metasurfaces have been utilized to achieve various Kerker conditions, and

thus are a versatile scattering platform to investigate a multitude of exotic and tunable scattering responses [24–27].

More recently, the so-called generalized Kerker effects on lossless all-dielectric resonators were studied, and it was shown that it is possible to achieve suppression of both forward and backward scattering through control of the interference between electric dipoles and off-resonance quadrupoles [25,28]. Although the requirement on the polarizabilities for perfect absorption [27] and achievement of both Kerker conditions simultaneously in lossless systems with multipoles has been studied [28], the full range of scattering states produced by lossy all-dielectric resonating systems, and the connection to their polarizabilities has not been well established. Here, we formalize the conditions necessary to achieve both zero backward and zero forward scattering simultaneously for a lossy all-dielectric metasurface, which – as we show – is equivalent to the so-called invisible metasurface [29–37]. Through subsequent modification of only the second Kerker condition, we find a state of perfect absorption [38], which is achieved by destructive interference of the radiated far-fields of the induced electric and magnetic dipole moments in all directions. Notably, the metasurface switches between states of absorptive and invisibility properties with only a change in resonator height – although a change in operational frequency results. We fabricate and characterize an infrared all-dielectric metasurface which achieves the first Kerker condition, and a modified second Kerker condition where the forward scattered wave exactly cancels the incident forward transmitted wave. We begin by considering the conditions on the electric polarizability (α) and magnetic polarizability (χ) necessary to achieve zero back scattering, defined as $S(\theta = \pi) = 0 \equiv S_\pi$, and zero forward scattering $S(\theta = 0) = 0 \equiv S_0$. In past work [23,39] only contributions from dipoles were considered, and it was found that S_π requires $\tilde{\alpha} = \tilde{\chi}$, and S_0 requires $\tilde{\alpha} = -\tilde{\chi}$, where the tilde denotes complex variables. Thus, if we desire a scatterer or scattering system that simultaneously achieves both Kerker conditions of zero back scattering and zero forward scattering, we must have that,

$$S_\pi \, \& \, S_0 \leftarrow \tilde{\alpha} = \tilde{\chi} = 0. \tag{1}$$

Therefore, strictly speaking, only a lossless material can simultaneously achieve both Kerker conditions.

Although the condition for S_0 requires $\tilde{\alpha} = -\tilde{\chi}$, it should be noted that the total wave in the forward direction S_T consists of the incident wave S_i and the forward scattered component (S_f), i.e. $S_T = S_i + S_f$. Thus in order to achieve a state of $S_T = 0$ it is necessary to establish a forward scattered wave S_f that is out-of-phase with S_i for complete destructive interference. We calculate the conditions on the complex dipole polarizabilities necessary to achieve several scattering cases including: S_0, S_π, $S_\pi \, \& \, S_0$, and $S_\pi \, \& \, S_T = 0$, the latter two of which we will show are equivalent to invisibility and perfect absorption, respectively, in all-dielectric metasurfaces.

Our all-dielectric metasurface consists of silicon cylindrical resonators arranged in a 2D hexagonal lattice, as depicted in Fig. 1(a). The hexagonal unit-cell was chosen in order to provide improved mechanical support to the free-standing metasurface, compared to a square unit-cell. In order to eliminate any substrate induced asymmetry, we use interconnects between unit cells in order to support the metasurface, as shown in Fig. 1(b). We chose a target frequency of 25 THz (12 μm wavelength), and we perform S-parameters simulations of the hexagonal metasurface array – see Supplement 1 for details. The metasurface (simulation only) has a radius of $r = 2.62$ μm, height $h_{pa} = 2.22$ μm and periodicity of p = 9.8 μm. In Fig. 2 (a), the simulated frequency dependent absorptivity (red) shows a peak absorptivity ($A(\omega)$) of 99.76% at a frequency of $\omega_0 = 25$ THz. The invisible metasurface is obtained with a change in height to $h_{ar} = 0.6 \mu$m, and $A(\omega)$, $R(\omega)$, and $T(\omega)$, are shown in Fig. 2(c). The invisible metasurface achieves near zero reflectance at 33.25 THz, $R = 0.068\%$, and a transmittance peak of 95.2% at 33.6 THz. The fabrication of the metasurface is provided in Supplement 1. We find an experimental peak absorptivity of 87% at 25.7 THz (Fig. 2(b)), and the width of the experimental $A(\omega)$ is broader than that predicted

by simulation, but overall the results match simulation relatively well. The simulated *A*, *R*, and *T* shown in Fig. 2(a) of the metasurface array indicate that the condition of simultaneous zero backward scattering and zero total forward scattering have been achieved.
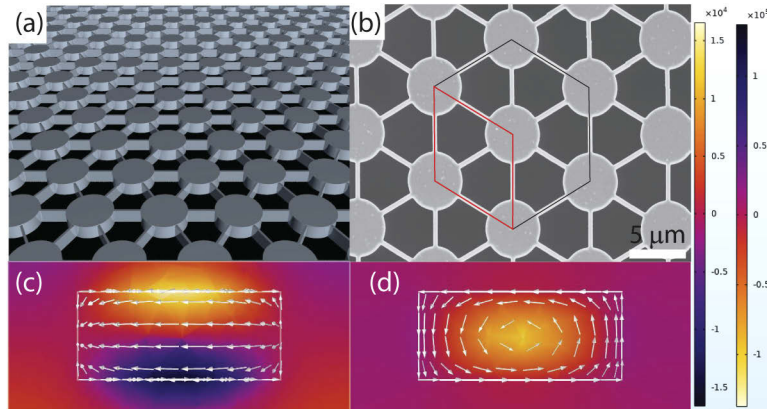

Fig. 1. (a) Schematic of the free standing infrared Kerker metasurface. SEM image of the fabricated metasurface (b), with dimensions of: r = 2.52 μm, h = 2.17 μm, interconnect width w = 400 nm, and periodicity *p* = 9.3 μm. Red lines denote the hexagonal unit-cell. (c) Even and (d) odd mode supported by the Kerker metasurface. White arrows denote the electric field vector, and the colormap shows the magnetic field vector, both at the frequency of peak absorptivity. Left (right) colorbar is for the even (odd) mode.
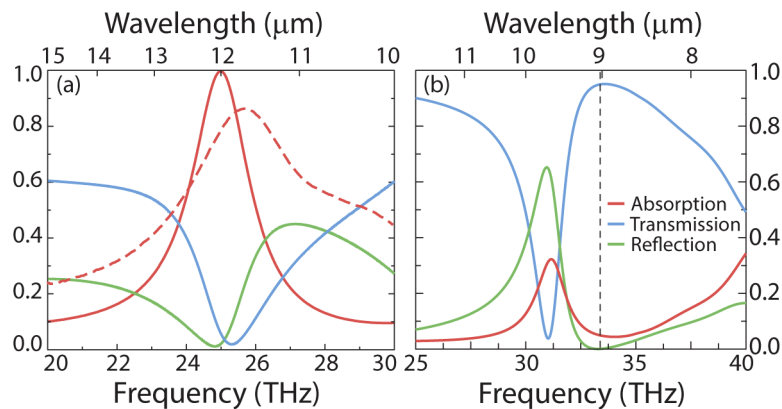

Fig. 2. (a) Simulated and experimental absorptivity (red and dashed red respectively), transmissivity (blue), and reflectivity (green) spectra of the absorber. The simulated absorber achieves *A* = 99.76 % at 25 THz, and has dimensions: *r* = 2.62 μm, h = 2.22 μm and periodicity of p = 9.8 μm. (b) Simulated invisible metasurface with dimensions the same as in (a), but with a height of h = 0.6 μm. Dashed vertical line indicates minimum reflectance of 0.068% at 33.25 THz.

The electric polarizability (α) and magnetic polarizability (χ), may be obtained from a multipole method (see Supplement 1) [5,40]. The metasurfaces we explore here are sub-wavelength, and thus we may approximate them as dipoles. The normalized electric and magnetic polarizabilities are given by $\alpha_n = \alpha/(\epsilon_0 V)$ and $\chi_n = \chi/V$, respectively, where α and χ are given in Eqs. S48 and S49, respectively, in Supplement 1, *V* is the volume of a single cylindrical resonator, and ϵ_0 is the permittivity of vacuum [41]. In Fig. 3 we show $\alpha_n(\omega)$ and $\chi_n(\omega)$ as the

red and blue curves, respectively, obtained from simulation for an array of free-standing silicon disks without interconnects. Two distinct metasurfaces are investigated, the perfect absorber shown in Fig. 3(a) and (b), and that of the invisible metasurface shown in Fig. 3(c) and (d). The real parts of the polarizabilities are plotted as solid curves, and the imaginary parts as dashed lines, where $\tilde{\alpha}_n = \alpha_{1,n} + i\alpha_{2,n}$, and $\tilde{\chi} = \chi_{1,n} + i\chi_{2,n}$. The polarizabilities of the absorber exhibit resonant behavior within the frequency range plotted, and we find that both $\alpha_{1,n}$ and $\chi_{1,n}$ achieve negative values, with zero crossing near 25 THz (dashed vertical grey line) – see Fig. 3(a), while the imaginary parts are approximately equal, as shown by the dashed vertical grey line at $\omega_0 = 25$ THz ($\lambda_0 = 12\mu m$) in Fig. 3(b). The polarizabilities of the invisible metasurface also exhibit resonant behavior, and we find that both $\alpha_{1,n}$ and $\alpha_{2,n}$ (red curves) shown in Fig. 3 (c) and (d) are approximately zero at 33.25 THz (dashed vertical grey line), while the imaginary parts (blue curves) are approximately zero across the range plotted in Fig. 3(c) and (d).
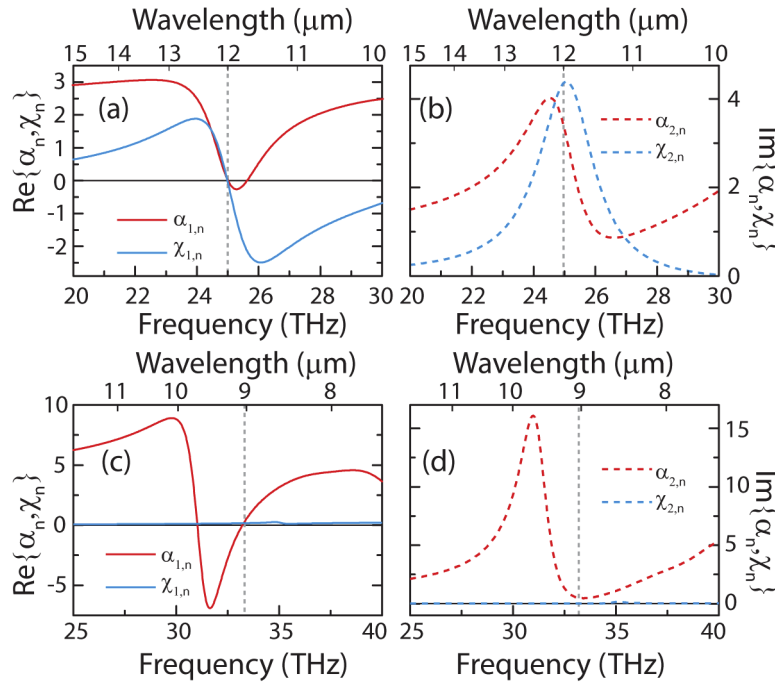

Fig. 3. Real (a) and imaginary (b) portions of the normalized electrical polarizability α_n (red colors), and normalized magnetic polarizability χ_n (blue colors) of the perfect absorber. Real (c) and imaginary (d) portions of the normalized polarizabilities of the invisible Kerker metasurface.

We next discuss the scattering and absorption cross sections. The absorption cross section (σ^{abs}), and the scattering cross section (σ^{sct}) may be determined directly from the polarizabilities. The extinction cross sectional scattering $\sigma^{ext} = \sigma^{sct} + \sigma^{abs}$ may have contributions from α and χ given by [42],

$$\sigma^{abs} = \sigma_\alpha^{abs} + \sigma_\chi^{abs} = \frac{k}{\varepsilon_0}\alpha_2 + k\chi_2 \tag{2}$$

$$\sigma^{sct} = \sigma_\alpha^{sct} + \sigma_\chi^{sct} = \frac{k^4}{6\pi\varepsilon_0^2}|\alpha|^2 + \frac{k^4}{6\pi}|\chi|^2 \tag{3}$$

where k is the free-space wavevector. In what follows, specific values are calculated and presented for the perfect absorber, and the invisible metasurface case is discussed in Supplement 1. Both

σ^{sct} and σ^{abs} are shown in Fig. 4 (a) and (b), due to either α (orange), or to χ (green). We find that σ^{sct} due to α and χ, (Fig. 3(a) and (b)), are approximately equal at ω_0, with values of $\sigma^{sct} \approx 140 \ \mu m^2$. The same is true of σ^{abs} due to α and χ, with values of $\sigma^{abs} \approx 100 \ \mu m^2$. In Fig. 4(c) we plot the σ^{sct}, and σ^{abs}, and in (d) the total extinction σ^{ext}. We note that the calculated cross sections shown in Fig. 4 are for a single unit-cell.
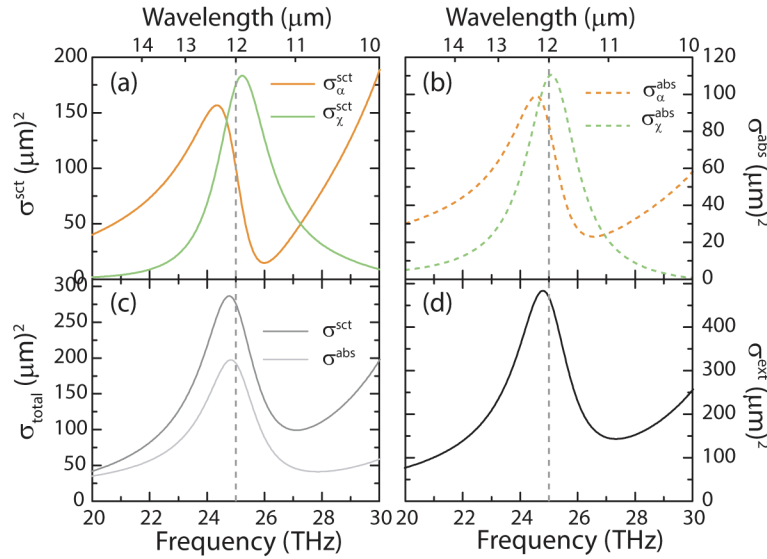

Fig. 4. (a) Frequency dependent scattering cross section (a) and absorption cross section (b) for α (orange) and χ (green). (c) Total scattering cross section (dark grey) and total absorption cross section (light grey). (d) Extinction cross section.

Powerflow unit-cell simulations for both Kerker metasurfaces is shown in Fig. 5 and highlights differences. In the perfect absorber, Fig. 5(a), all powerflow streamlines at ω_0 and are pulled into the resonator and form a family of inward Lituus-type spirals [43] that wind to asymptotic singular points (see Visualization 1) – the so-called optical vortices [44,45]. We find that for the case of the invisible metasurface, (Fig. 5(b)), power incident (from the left) in one unit-cell at 33.25 THz, that the majority of streamlines exit to the right – in accord with the transmission shown in Fig. 2(b). We also observed that at 33.25 THz, the transmitted phase from the metasurface was the same as that with metasurface replaced by free space, (not shown). It can be observed that a few are captured by the metasurface, and these represent σ^{abs}. Distortion of the streamlines is due to interference from imperfect S_0 and S_π. The solid black streamline denotes the separatrix between those streamlines which are absorbed and those that are not.

We formalize the relation between the scattering cross sections and the loss rates of a passive system. The absorption of an all-dielectric metasurface can be described by absorption arising from electric and magnetic resonances [46]. If the resonances are degenerate, the absorption at resonance is determined by the ratio of the material loss rate (δ) to the radiative loss rate (γ), which is proportional to the ratio of σ^{abs} to σ^{sct}, i.e. $\eta \equiv \sigma^{abs}/\sigma^{sct} \propto \delta/\gamma$ [47]. The absorptivity shown in Fig. 2(a) achieves $A = 99.76\%$ at ω_0, and is usually under the condition of critical coupling, i.e. a balance which dictates that the radiative loss rate γ is equal to the material loss rate δ. Since the scattering cross section is proportional to γ and the absorption cross section is proportional to δ, we may estimate the peak absorptivity at ω_0 using coupled mode theory (CMT). For a system consisting of two resonances, CMT describes the absorptivity as (see Supplement
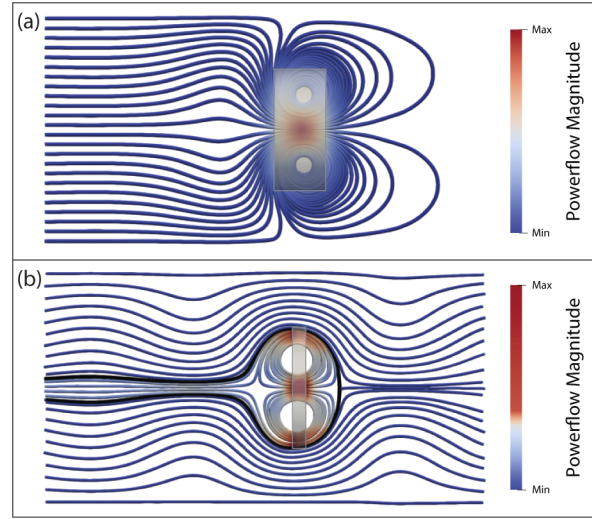
Fig. 5. Simulated power flow for two all-dielectric metasurfaces which achieve (a) the first Kerker condition and the modified second Kerker condition given by Eq. (7), and (b) the both Kerker conditions simultaneously given by Eq. (1)

1),

$$A(\omega_0) = \frac{2\eta_1}{(\eta_1 + 1)^2} + \frac{2\eta_2}{(\eta_2 + 1)^2} \tag{4}$$

where subscripted 1's and 2's denote the resonances due to α and χ, respectively. Using the four scattering cross sectional values shown in Fig. 4(a) and (b) at ω_0 in Eq. (4), we calculate $A = 97.0\%$, which is close to the simulated value, with a percent error of 2.8%. Although we do not perfectly achieve critical coupling, i.e. $\sigma^{abs} < \sigma^{sct} \rightarrow \eta \approx 0.70$, see Fig. 4 (c), A is robust to differences in radiative scattering and absorption, and Eq. (4) indicates that we can still acquire high absorptivity values of $A \geq 95\%$ for $0.635 \leq \eta \leq 1.576$ [46].

Forms for the polarizability dependent reflectivity coefficient (r) and transmissivity coefficient (t) at normal incidence, and which take into account Fano interference due to the array, are derived in Supplement 1 and given by,

$$\tilde{r} = \frac{ik\rho}{2}(\tilde{\alpha} - \tilde{\chi}) \tag{5}$$

$$\tilde{t} = 1 + \frac{ik\rho}{2}(\tilde{\alpha} + \tilde{\chi}) \tag{6}$$

where ρ is the density of dipoles per unit area, and k is the free space wavevector. Evaluating Eq. (5) for $r = 0$ gives, $\tilde{r} = 0 \leftarrow \tilde{\alpha} = \tilde{\chi}$, which is in accord with Kerker's first condition. Under the second modified Kerker condition, in which t should go to zero, we find a relation for the real and imaginary polarizabilities given by Eq. (6) as, $\tilde{t} = 0 \leftarrow \{\alpha_1 + \chi_1 = 0, \alpha_2 + \chi_2 = 2/k\rho\}$.

We see that in order to obtain $r = 0$ requires that the complex polarizabilities be equal, but for $t = 0$ the real parts should sum to zero. Thus for $r = t = 0$ it is required that real portions of the polarizabilities be equal to zero – in accord to that prescribed by the Kerker conditions – and the imaginary polarizabilities must be equal to each other, giving [27,48],

$$\tilde{r} = \tilde{t} = 0 \leftarrow \begin{cases} \alpha_1 = \chi_1 = 0 \\ \alpha_2 = \chi_2 = \frac{1}{k\rho} \end{cases} \tag{7}$$

Evaluating α_2 and χ_2 in Eq. (7) with $k = 2\pi/\lambda$, with $\rho = 1/A_{pc}$ where A_{pc} is the area of the primitive unit-cell and $\lambda_0 = 12\mu m$, we find the normalized imaginary polarizabilities, i.e. $\alpha_{2,n} = \chi_{2,n} = (Vk\rho)^{-1}$, give $\alpha_{2,n} = \chi_{2,n} = 3.83$. Notably, the imaginary polarizabilities determined with only dipole contributions (Fig. 3(b)) cross near $\lambda_0 = 12\mu m$ (ω_0), and are close to values predicted from Eq. (7) – we find an average value of $(\alpha_{2,n} + \chi_{2,n})/2 = 3.84$. The asymmetry parameter is defined as the average of the cosine of the scattering angle g=$\langle\cos\theta\rangle$, and is given in terms of dipole polarizabilities as, g=$Re[\alpha\chi^*]/(|\alpha|^2 + |\chi|^2)$ [49,50]. For the S_π & S_0 state, the asymmetry parameter is defined to be zero. The frequency dependence of $g(\omega)$ is shown in Fig. S1 of Supplement 1 for the perfect absorber (g_{pa}) and invisible metasurface (g_{ar}) and we find excellent agreement with theoretical predicted values, i.e. $g_{pa} = 0.48$ and $g_{ar} = 0.07$ for each, respectively, shown in Table 1 in the g_* column. Conditions on the polarizabilities and g-parameters needed for the first and second Kerker conditions, simultaneous Kerker conditions, $r = 0$, $t = 0$, and perfect absorption are summarized in Table 1.

Table 1. Conditions on the dipole polarizabilities to achieve various scattering states, and the corresponding asymmetry parameter (g). The quantity g_t is defined in Supplement 1, and the g_* column denotes values found in this study.

Scattered State	Re[$\tilde{\alpha}, \tilde{\chi}$]	Im[$\tilde{\alpha}, \tilde{\chi}$]	g	g_*
First Kerker Condition / Zero Reflectance ($S_\pi, r = 0$)	$\alpha_1 = \chi_1$	$\alpha_2 = \chi_2$	1/2	-
Second Kerker Condition (S_0)	$\alpha_1 = -\chi_1$	$\alpha_2 = -\chi_2$	-1/2	-
Both Kerker Conditions / Invisibility (S_π & S_0)	$\alpha_1 = \chi_1 = 0$	$\alpha_2 = \chi_2 = 0$	$\equiv 0$	0.07
Zero Transmittance ($t = 0$)	$\alpha_1 = -\chi_1$	$\alpha_2 + \chi_2 = \frac{2}{k\rho}$	g_t	-
Perfect Absorption ($r = t = 0$)	$\alpha_1 = \chi_1 = 0$	$\alpha_2 = \chi_2 = \frac{1}{k\rho}$	1/2	0.48

We have detailed conditions necessary to realize both Kerker conditions simultaneously in all-dielectric metasurfaces. Although forward scattering is strongly suppressed, due to materials loss it can never reach zero, and thus there is no violation of the optical theorem [51]. We have further specified the similar but distinct requirements for a modified second Kerker condition in terms of the polarizabilities. The polarizabilities we show here are calculated using only dipole terms and match well to the Kerker description of the all-dielectric metasurfaces — summarized in Table 1 — which assumes only dipole polarizabilities. Supplement 1 explores scattering cross sections due to the higher order multipoles, and we find that they possess relatively small values at the operational frequency of the perfect absorber. However, in the case of the invisible metasurface, we find that scattering due to the toroidal dipole increases with increasing frequency, and crosses the electric dipole curve near 33.25 THz. The resulting anapole may thus be used to explain the zero scattering in the forward direction. Although the invisible metasurface may be understood considering higher order multiples, the polarizability values shown in Fig. 3, however, match Table 1 well. It thus appears that a strictly dipole-only polarizability is compatible with the Kerker description, but one may also chose to disentangle contributions to the polarizabilities due to toroidal dipoles. The calculated scattered cross sections and absorption cross sections are well described by coupled mode theory, and verify that absorption occurs by degenerate critical coupling.

Disclosures. The authors declare no conflicts of interest.

Supplemental document. See Supplement 1 for supporting content.

References

1. M. Kerker, *The scattering of light and other electromagnetic radiation* (Acad. Press, 1987).
2. A. Zangwill, *Modern Electrodynamics* (Cambridge University Press, 2012).
3. I. M. Hancu, A. G. Curto, M. Castro-López, M. Kuttge, and N. F. van Hulst, "Multipolar Interference for Directed Light Emission," Nano Lett. **14**(1), 166–171 (2014).
4. I. Staude, A. E. Miroshnichenko, M. Decker, N. T. Fofang, S. Liu, E. Gonzales, J. Dominguez, T. S. Luk, D. N. Neshev, I. Brener, and Y. Kivshar, "Tailoring directional scattering through magnetic and electric resonances in subwavelength silicon nanodisks," ACS Nano **7**(9), 7824–7832 (2013).
5. A. E. Miroshnichenko, A. B. Evlyukhin, Y. F. Yu, R. M. Bakker, A. Chipouline, A. I. Kuznetsov, B. Luk'yanchuk, B. N. Chichkov, and Y. S. Kivshar, "Nonradiating anapole modes in dielectric nanoparticles," Nat. Commun. **6**(1), 8069 (2015).
6. W. Liu and A. E. Miroshnichenko, "Beam steering with dielectric metalattices," ACS Photonics **5**(5), 1733–1741 (2018).
7. S. Kruk and Y. Kivshar, "5-tailoring transmission and reflection with metasurfaces," in *Dielectric Metamaterials*, I. Brener, S. Liu, I. Staude, J. Valentine, and C. Holloway, eds. (Woodhead Publishing, 2020), Woodhead Publishing Series in Electronic and Optical Materials, pp. 145–174.
8. C. Pfeiffer and A. Grbic, "Metamaterial huygens' surfaces: Tailoring wave fronts with reflectionless sheets," Phys. Rev. Lett. **110**(19), 197401 (2013).
9. M. Decker, I. Staude, M. Falkner, J. Dominguez, D. N. Neshev, I. Brener, T. Pertsch, and Y. S. Kivshar, "High-efficiency dielectric huygens' surfaces," Adv. Opt. Mater. **3**(6), 813–820 (2015).
10. D. Arslan, K. E. Chong, A. E. Miroshnichenko, D.-Y. Choi, D. N. Neshev, T. Pertsch, Y. S. Kivshar, and I. Staude, "Angle-selective all-dielectric huygens' metasurfaces," J. Phys. D: Appl. Phys. **50**(43), 434002 (2017).
11. K. Fan, J. Zhang, X. Liu, G.-F. Zhang, R. D. Averitt, and W. J. Padilla, "Phototunable dielectric huygens' metasurfaces," Adv. Mater. **30**(22), 1800278 (2018).
12. A. I. Kuznetsov, A. E. Miroshnichenko, M. L. Brongersma, Y. S. Kivshar, and B. Luk'yanchuk, "Optically resonant dielectric nanostructures," Science **354**(6314), aag2472 (2016).
13. Y. Yang, W. Wang, P. Moitra, I. I. Kravchenko, D. P. Briggs, and J. Valentine, "Dielectric meta-reflectarray for broadband linear polarization conversion and optical vortex generation," Nano Lett. **14**(3), 1394–1399 (2014).
14. Y. Yifat, M. Eitan, Z. Iluz, Y. Hanein, A. Boag, and J. Scheuer, "Highly efficient and broadband wide-angle holography using patch-dipole nanoantenna reflectarrays," Nano Lett. **14**(5), 2485–2490 (2014).
15. D. Headland, E. Carrasco, S. Nirantar, W. Withayachumnankul, P. Gutruf, J. Schwarz, D. Abbott, M. Bhaskaran, S. Sriram, J. Perruisseau-Carrier, and C. Fumeaux, "Dielectric resonator reflectarray as high-efficiency nonuniform terahertz metasurface," ACS Photonics **3**(6), 1019–1026 (2016).
16. J. Y. Suen, K. Fan, and W. J. Padilla, "A zero-rank, maximum nullity perfect electromagnetic wave absorber," Adv. Opt. Mater. **7**(8), 1801632 (2019).
17. W. Zhu, F. Xiao, M. Kang, and M. Premaratne, "Coherent perfect absorption in an all-dielectric metasurface," Appl. Phys. Lett. **108**(12), 121901 (2016).
18. X. Feng, J. Zou, W. Xu, Z. Zhu, X. Yuan, J. Zhang, and S. Qin, "Coherent perfect absorption and asymmetric interferometric light-light control in graphene with resonant dielectric nanostructures," Opt. Express **26**(22), 29183–29191 (2018).
19. K. Koshelev, S. Lepeshov, M. Liu, A. Bogdanov, and Y. Kivshar, "Asymmetric metasurfaces with high-*q* resonances governed by bound states in the continuum," Phys. Rev. Lett. **121**(19), 193903 (2018).
20. A. S. Kupriianov, Y. Xu, A. Sayanskiy, V. Dmitriev, Y. S. Kivshar, and V. R. Tuz, "Metasurface engineering through bound states in the continuum," Phys. Rev. Appl. **12**(1), 014024 (2019).
21. K. Fan, I. V. Shadrivov, and W. J. Padilla, "Dynamic bound states in the continuum," Optica **6**(2), 169–173 (2019).
22. K. Koshelev, A. Bogdanov, and Y. Kivshar, "Meta-optics and bound states in the continuum SPECIAL TOPIC: Electromagnetic Metasurfaces: from Concept to Applications," Sci. Bull. **64**(12), 836–842 (2019).
23. M. K. D.-S. Wang and C. L. Giles, "Electromagnetic scattering by magnetic spheres," J. Opt. Soc. Am. **73**(6), 765–767 (1983).
24. V. E. Babicheva and A. B. Evlyukhin, "Resonant lattice kerker effect in metasurfaces with electric and magnetic optical responses," Laser Photonics Rev. **11**(6), 1700132 (2017).
25. W. Liu and Y. S. Kivshar, "Generalized kerker effects in nanophotonics and meta-optics [invited]," Opt. Express **26**(10), 13085–13105 (2018).
26. N. Odebo Länk, R. Verre, P. Johansson, and M. Käll, "Large-scale silicon nanophotonic metasurfaces with polarization independent near-perfect absorption," Nano Lett. **17**(5), 3054–3060 (2017).
27. J. Si, X. Yu, J. Zhang, W. Yang, S. Liu, and X. Deng, "Broadened band near-perfect absorber based on amorphous silicon metasurface," Opt. Express **28**(12), 17900–17905 (2020).
28. H. K. Shamkhi, K. V. Baryshnikova, A. Sayanskiy, P. Kapitanova, P. D. Terekhov, P. Belov, A. Karabchevsky, A. B. Evlyukhin, Y. Kivshar, and A. S. Shalin, "Transverse scattering and generalized kerker effects in all-dielectric mie-resonant metaoptics," Phys. Rev. Lett. **122**(19), 193905 (2019).
29. M. V. Rybin, D. S. Filonov, P. A. Belov, Y. S. Kivshar, and M. F. Limonov, "Switching from Visibility to Invisibility via Fano Resonances: Theory and Experiment," Sci. Rep. **5**(1), 8774 (2015).

30. M. V. Rybin, K. B. Samusev, P. V. Kapitanova, D. S. Filonov, P. A. Belov, Y. S. Kivshar, and M. F. Limonov, "Switchable invisibility of dielectric resonators," Phys. Rev. B **95**(16), 165119 (2017).

31. Y. Kobayashi and K. Kajikawa, "Homogeneous dielectric cylinders invisible at optical frequency," Appl. Phys. Express **12**(4), 042001 (2019).

32. V. E. Babicheva, M. I. Petrov, K. V. Baryshnikova, and P. A. Belov, "Reflection compensation mediated by electric and magnetic resonances of all-dielectric metasurfaces [invited]," J. Opt. Soc. Am. B **34**(7), D18–D28 (2017).

33. L. Huang, C.-C. Chang, B. Zeng, J. Nogan, S.-N. Luo, A. J. Taylor, A. K. Azad, and H.-T. Chen, "Bilayer Metasurfaces for Dual- and Broadband Optical Antireflection," ACS Photonics **4**(9), 2111–2116 (2017).

34. A. K. Ospanova, A. Karabchevsky, and A. A. Basharin, "Metamaterial engineered transparency due to the nullifying of multipole moments," Opt. Lett. **43**(3), 503 (2018).

35. H.-T. Chen, J. Zhou, J. F. O'Hara, F. Chen, A. K. Azad, and A. J. Taylor, "Antireflection coating using metamaterials and identification of its mechanism," Phys. Rev. Lett. **105**(7), 073901 (2010).

36. P. D. Terekhov, V. E. Babicheva, K. V. Baryshnikova, A. S. Shalin, A. Karabchevsky, and A. B. Evlyukhin, "Multipole analysis of dielectric metasurfaces composed of nonspherical nanoparticles and lattice invisibility effect," Phys. Rev. B **99**(4), 045424 (2019).

37. A. Karabchevsky, E. Falek, Y. Greenberg, M. Elman, Y. Keren, and I. Gurwich, "Broadband transparency with all-dielectric metasurfaces engraved on silicon waveguide facets: effect of inverted and extruded features based on babinet's principle," Nanoscale Adv. **2**(7), 2977–2985 (2020).

38. N. I. Landy, S. Sajuyigbe, J. J. Mock, D. R. Smith, and W. J. Padilla, "Perfect metamaterial absorber," Phys. Rev. Lett. **100**(20), 207402 (2008).

39. J. Y. Lee, A. E. Miroshnichenko, and R.-K. Lee, "Simultaneously nearly zero forward and nearly zero backward scattering objects," Opt. Express **26**(23), 30393–30399 (2018).

40. P. D. Terekhov, K. V. Baryshnikova, Y. A. Artemyev, A. Karabchevsky, A. S. Shalin, and A. B. Evlyukhin, "Multipolar response of nonspherical silicon nanoparticles in the visible and near-infrared spectral ranges," Phys. Rev. B **96**(3), 035443 (2017).

41. A. Sihvola, "Dielectric Polarization and Particle Shape Effects," J. Nanomater. **2007**, 1–9 (2007).

42. S. Tretyakov, "Maximizing Absorption and Scattering by Dipole Particles," Plasmonics **9**(4), 935–944 (2014).

43. J. D. Lawrence, *A catalog of special plane curves* (Dover Publications, 2014).

44. A. A. Andronov, A. A. Vitt, and S. E. Chajkin, *Theory of oscillators* (Dover Publ., 2014).

45. M. V. Bashevoy, V. A. Fedotov, and N. I. Zheludev, "Optical whirlpool on an absorbing metallic nanoparticle," Opt. Express **13**(21), 8372–8379 (2005).

46. X. Ming, X. Liu, L. Sun, and W. J. Padilla, "Degenerate critical coupling in all-dielectric metasurface absorbers," Opt. Express **25**(20), 24658–24669 (2017).

47. Z. Ruan and S. Fan, "Temporal coupled-mode theory for light scattering by an arbitrarily shaped object supporting a single resonance," Phys. Rev. A **85**(4), 043828 (2012).

48. A. B. Evlyukhin, C. Reinhardt, A. Seidel, B. S. Luk'yanchuk, and B. N. Chichkov, "Optical response features of si-nanoparticle arrays," Phys. Rev. B **82**(4), 045404 (2010).

49. J. Olmos-Trigo, D. R. Abujetas, C. Sanz-Fernández, J. A. Sánchez-Gil, and J. J. Sáenz, "Optimal backward light scattering by dipolar particles," Phys. Rev. Research **2**(1), 013225 (2020).

50. C. F. Bohren and D. R. Huffman, *Absorption and scattering of light by small particles* (Wiley-VCH, 2009).

51. A. Alu and N. Engheta, "How does zero forward-scattering in magnetodielectric nanoparticles comply with the optical theorem?" J. Nanophotonics **4**, 1–18 (2010).